J. of Electromagn. Waves and Appl., Vol. 11.

PHASE-SPACE BEAM SUMMATION: A LOCAL SPECTRUM ANALYSIS OF TIME-DEPENDENT RADIATION

Timor Melamed

Tel-Aviv University, Faculty of Engineering, Dept. of Electrical Engineering – Physical Electronics, Tel-Aviv 69978, Israel

Abstract—The phase-space beam summation is a general analytical framework for local analysis and modeling of radiation from extended source distributions. In this formulation the field is expressed as a superposition of beam propagators that emanate from all points in the source domain and in all directions. The theory is presented here for both time-harmonic and time-dependent fields: in the later case, the propagators are pulsed-beams (PB). The phase-space spectrum of beam propagators is matched locally to the source distribution via local spectral transforms: a local Fourier transform for time-harmonic fields and a "local Radon transform" for time-dependent fields. These transforms extract the local radiation properties of the source distributions and thus provide a priori localized field representations. Some of these basic concepts have been introduced previously for two-dimensional configurations. The present paper extends the theory to three dimensions, derives the operative expressions for the transforms and discusses additional phenomena due to the three dimensionality. Special emphasis is placed on numerical implementation and on choosing a numerically converging space-time window. It is found that the twice differentiated Gaussian-δ window is both properly converging and provides a convenient propagator that that can readily be tracked in complicated inhomogeneous medium.

I. INTRODUCTION

The radiation and analysis of short pulse fields are receiving increased attention for various applications, e.g., synthesis of high energy wavepackets, target interrogation, environmental sensing and inverse scattering. Of particular interest for these applications are collimated short-pulse fields (space-time wavepackets) [1–6]. Because of the wide frequency band of such fields, the conventional route of inversion of frequency-domain (FD) solutions is often less convenient and physically less transparent than direct treatment in the time domain (TD) where the wave events are well localized. This paper is therefore concerned with field representations directly in the time domain, with emphasis on local spectrum representations. *Localization* of wave phenomena is of fundamental significance because local models can be adapted to *complicated global* events provided that the scale of complexity is large in comparison with the local domain. Ray-based localization provide an effective parametrization but they are limited to smooth field structures. They are ineffective, though, in many situations, such as transition regions, long observation times or spectrally rich sources, in which cases one should resort to spectral representations that can accommodate the richer spectral content of the wave.

The conventional spectral elements for wave synthesis are Green's functions or plane waves [7] (the generic name plane-waves should be understood in a generalized sense for inhomogeneous medium configurations [8]; it is also used here to denote time-dependent plane waves [9–12]). However, tracking these *global* basis functions in inhomogeneous environments or through interactions with objects is complicated, and the resulting representation integrals are spectrally distributed. Invoking constructive interference yields local observables in the form of ray fields, but as mentioned above, in many situations a wider spectral range of basis functions is required [8].

Instead of using *global* basis functions that lead to distributed integrals, the representation may be localized *a priori* by using beams as *local* basis wave-functions (the term "beam" is used conventionally for collimated time-harmonic waves; here we use it as a generic term also for "pulsed-beams" which are collimated time-dependent wavepackets [5]). Each beam basis function then accounts collectively for the radiation from a finite region in the source domain, thereby leading to compact spectral representations. Further compactization is due to the fact that only those beams that pass near the space-time observation point actually contribute there. Finally, the beam propagators can be tracked locally in complicated medium and are insensitive to transition regions and caustics [13].

The pulsed-beam basis functions considered here belong to the general class of the complex source pulsed-beam [5]. In addition to providing a complete set of basis function for several types of expansion (see discussion below) they have other favorable properties for modeling collimated wavepacket propagation in homogeneous or in inhomogeneous media [13] and for analysis of local scattering and diffraction phenomena [14, 15]

Several beam expansion schemes have been introduced recently.

They may be grouped in three categories. For *point source* configurations the source field can be expanded into an angular spectrum of beams that emanate from the source in all directions. This approach has been applied heuristically for time-harmonic fields [16], and later [17] it has been extended to time-dependent fields and justified as an *exact* identity.

A different class of expansions applies for *extended source* configurations. It involves a spectrum of shifted and tilted beams which emanate in all directions from all points in the source domain. The beam amplitudes are determined by the local spectrum of the source. Several alternative formulations for time-harmonic [18–23] and time-dependent [24–26] fields have been introduced: In [20, 24–26] and also in [23] they have been placed within a unified phase-space format wherein a phase-space distribution of beam propagators are *locally* matched to the source distribution.

Alternatively, *well collimated* sources have been expanded by means of a *global* approach. Here, greater efficiency is achieved by matching wide beam basis functions to the entire source distribution so that each of them now exhibits the global collimation properties of the source with respect to near to far zone transition. This approach have been formulated first in the FD [27] but more recently it has been extended to the TD [28]. A forth beam expansion strategy for marching of fields in a guiding environment has been introduced recently in [29].

The present paper is concerned with the phase-space scheme mentioned above, which is a general mathematical framework for local synthesis of radiation from extended source distributions. In this approach the phase-space spectrum of local basis functions (beams) is matched locally to the source distribution via local spectral transforms: a windowed Fourier transform for time-harmonic fields [20] and the recently introduced "local Radon transform" for time-dependent fields [24, 26]. These transforms extract the local radiation properties of the source distributions, thereby emphasizing those beam basis functions that locally coincide with these properties (see Fig. 1). It is therefore particularly useful for spectrally rich distributions (e.g. local analysis and inverse scattering of short-pulse scattering data [30]).

The basic concepts of the phase-space representation have been introduced originally for 2D configurations [20, 24, 25]. The present paper extends the formulation to 3D and discusses additional phenomena that are incurred by the three dimensionality. This extension is essential in particular for time-dependent problems where the operators for 2D fields are inherently different than those for the physical 3D fields. Special emphasis is also placed here on the numerical implementation. This also involves choosing a properly

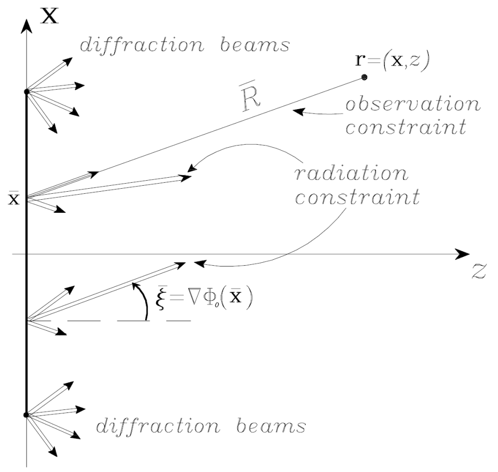

Figure 1. Phase-space beam (or pulsed-beam) summation for radiation from extended source distributions. The double arrows represent the beam propagators. Large arrows represent beams that are strongly excited by local features of the source distribution (i.e., geometrically enhanced beams).

converging space-time window function. It is found that the twice differentiated Gaussian-δ window is both properly converging and also provides a convenient propagator that has a closed form expression. Furthermore, this propagator is closely related to the general class of collimated pulsed-beam fields considered in [5] that can readily be tracked in complicated inhomogeneous medium [13]. This enables an efficient representation for the propagated field. Indeed, the local spectrum operation derived in this paper have subsequently been used for the analysis of scattering data and for inverse scattering [30].

Concerning the layout of presentation, we start with the plane-wave formulations in the FD and then in the TD (Sec. II). The TD formulation involves the slant-stack transform (SST) which is a Radon transform of the data in the space-time domain. We also discuss the conditions for a spectral localization of this distributed TD representation. Such localization is the counterpart of the high frequency stationary phase localization in the FD. The local spectrum formulations in the FD and TD are then described in general terms in Sec. III, while closed-form expressions for the phase-space transforms and propagators for specific choices of windows are given in Sec. IV. These windows are the Gaussian and the twice differentiated Gaussian-δ windows for FD and TD formulations, respectively. These windows not only provide convenient kernels for numerical processing, but they also yield convenient closed-form expressions for the propagators. Finally, numerical examples for time-dependent plane-wave spectrum and for time-dependent local spectrum analyses of a short-pulse field distribution are considered in Sec. V.

II. PLANE-WAVE SPECTRAL REPRESENTATIONS

We are concerned with the field $u(\mathbf{r}, t)$ radiated into the homogeneous half space $z > 0$ due to the time-dependent field distribution $u_o(\mathbf{x}, t)$ in the $z = 0$ plane. The adopted notations for the Cartesian coordinate frame are $\mathbf{r} = (x_1, x_2, z)$ and $\mathbf{x} = (x_1, x_2)$. We shall start with the analysis of the corresponding time-harmonic field $\widehat{u}(\mathbf{r}; \omega)$. We use over carets to denote time-harmonic field constituents, defined by the Fourier transform relations

$$\widehat{u}(\mathbf{r}, \omega) = \int_{-\infty}^{\infty} dt\, u(\mathbf{r}, t) e^{i\omega t}, \quad u(\mathbf{r}, t) = \frac{1}{2\pi} \int_{-\infty}^{\infty} d\omega\, \widehat{u}(\mathbf{r}; \omega) e^{-i\omega t} \tag{1 a,b}$$

The ω-dependence $\widehat{u}(\mathbf{r})|_\omega$ is suppressed for the frequency domain analysis. However, when inverting to the time domain, the frequency dependence of $\widehat{u}(\mathbf{r}; \omega)$ is exhibited explicitly.

II.1. Frequency-domain

The plane-wave spectral distribution of the initial field $\widehat{u}_o(\mathbf{x})$ is defined via

$$\widehat{\widehat{u}}_o(\boldsymbol{\xi}) = \int d^2x\, \widehat{u}_o(\mathbf{x})\, e^{-ik\boldsymbol{\xi}\cdot\mathbf{x}} \tag{2}$$

where, anticipating extension to the TD (Sec. II.2), the wavenumber vector $\boldsymbol{\xi} = (\xi_1, \xi_2)$ is normalized with respect to $k = \omega/v$ with v being the wave propagation speed in the medium. The plane-wave representation for the field is therefore

$$\widehat{u}(\mathbf{r}) = (k/2\pi)^2 \int d^2\xi\, \widehat{\widehat{u}}_o(\boldsymbol{\xi})\, e^{ik\,(\boldsymbol{\xi}\cdot\mathbf{x}+\zeta z)} \tag{3}$$

where

$$\zeta = \sqrt{1 - |\boldsymbol{\xi}|^2}, \qquad \mathrm{Im}\zeta \geq 0 \tag{4}$$

where we use $|\boldsymbol{\xi}|^2 = \boldsymbol{\xi} \cdot \boldsymbol{\xi}$. In the propagating spectrum domain $|\boldsymbol{\xi}| < 1$, the integral (3) consists of real plane-waves $e^{ik\boldsymbol{\kappa}\cdot\mathbf{r}}$ where the unit vector $\boldsymbol{\kappa} = (\boldsymbol{\xi}, \zeta)$ is the propagation direction. In the evanescent spectrum region $|\boldsymbol{\xi}| > 1$, the plane-waves decay exponentially away from the $z = 0$ plane.

II.2. Time domain

II.2.1. Analytic signals

The TD field formulations will be derived by transforming the FD formulations. In order to gain flexibility in the derivation, in particular in those formulations that involve evanescent spectra, it will be convenient to use the analytic signal representation. The final results, however, will be expressed in terms of real signals.

The analytic signal $\overset{+}{u}(\mathbf{r}, t)$ associated with a real (physical) signal $u(\mathbf{r}, t)$ with frequency spectrum $\widehat{u}(\mathbf{r}; \omega)$ is defined via the one sided inverse Fourier transform

$$\overset{+}{u}(\mathbf{r}, t) = \frac{1}{\pi} \int_0^\infty d\omega \, e^{-i\omega t} \, \widehat{u}(\mathbf{r}; \omega), \quad \mathrm{Im} t \leq 0. \tag{5}$$

Henceforth, all analytic signals will be denoted with an over $+$. Clearly, the integral in (5) defines an analytic function in the lower half of the complex t-plane. The analytic signal may also be defined directly from the time-dependent data via

$$\overset{+}{u}(\mathbf{r}, t) = \frac{1}{\pi i} \int_{-\infty}^\infty dt' \frac{u(\mathbf{r}, t')}{t - t'}, \quad \mathrm{Im} t \leq 0. \tag{6}$$

Thus, the limit of the analytic on the real t-axis is related to the real signal $u(t)$ via

$$\overset{+}{u}(\mathbf{r}, t) = u(\mathbf{r}, t) + i\mathcal{H}u(\mathbf{r}, t), \quad t \text{ real} \tag{7}$$

where $\mathcal{H}$ in the Hilbert transform $\mathcal{H}u = (-\pi t)^{-1} \otimes u$ with $\otimes$ denoting a convolution, i.e.,

$$f(t) \otimes g(t) = \int dt' \, f(t' - t) g(t') \tag{8}$$

The real signal for real t is thus recovered via $u(\mathbf{r}, t) = \mathrm{Re}\, \overset{+}{u}(\mathbf{r}, t)$.

II.2.2. Analytic signals representation of the time-dependent plane-wave spectrum

With $u_o(\mathbf{x}, t)$ representing the time-dependent field in the $z = 0$ plane, the analytic transient plane-wave spectrum $\overset{+}{\widetilde{u}}_o(\boldsymbol{\xi}, \tau)$ is defined by

$$\overset{+}{\widetilde{u}}_o(\boldsymbol{\xi}, \tau) = \frac{1}{\pi} \int_0^\infty d\omega \, \widehat{\widetilde{u}}_o(\boldsymbol{\xi}; \omega) \, e^{-i\omega\tau}, \tag{9}$$

giving, using (2)

$$\overset{+}{\tilde{u}}_o(\boldsymbol{\xi},\tau)=\frac{1}{\pi}\int_0^\infty d\omega\int d^2x\;\widehat{u}_o(\mathbf{x};\omega)\;e^{-i\omega(\tau+v^{-1}\boldsymbol{\xi}\cdot\mathbf{x})}. \tag{10}$$

Note that an important feature of the spectral formulation in (2) is that the spatial wave number is normalized with respect to ω and thus has a frequency independent geometrical interpretation in terms of the plane-wave angle. Thus, inverting the order of integration in (10) (legitimate when $\mathrm{Im}t \le 0$ and in the limit of real t) and evaluating the ω-integration in closed form, one finds that the time-dependent spatial spectrum is found directly from the analytic data $\overset{+}{u}_o(\mathbf{x},t)$ via

$$\overset{+}{\tilde{u}}_o(\boldsymbol{\xi},\tau)=\int d^2x\;\overset{+}{u}_o(\mathbf{x},\tau+v^{-1}\boldsymbol{\xi}\cdot\mathbf{x}). \tag{11}$$

Repeating the same procedure for the field representation in (3) one obtains

$$\overset{+}{u}(\mathbf{r},t)=-(2\pi v)^{-2}\int d^2\xi\partial_t^2\;\overset{+}{\tilde{u}}_o[\boldsymbol{\xi},t-v^{-1}(\boldsymbol{\xi}\cdot\mathbf{x}+\zeta z)]. \tag{12}$$

and finally, the physical field is given by $u(\mathbf{r},t)=\mathrm{Re}\,\overset{+}{u}(\mathbf{r},t)$

Eq. (11) is a Radon transform of $u_o(\mathbf{x},t)$ in the three dimensional $(\mathbf{x},t)$ space, consisting of projections of $u_o(\mathbf{x},t)$ along surfaces of linear delay $t-v^{-1}\boldsymbol{\xi}\cdot\mathbf{x}=\tau=const.$ (Fig. 2). It has therefore been termed the *slant-stack* transform (SST) [9, 31]. It extracts from $u_o(\mathbf{x},t)$ the transient plane-wave signal that propagates in the direction $\boldsymbol{\kappa}=(\boldsymbol{\xi},\zeta)$. Eq. (12) indeed reconstructs the field in terms of an angular ($\boldsymbol{\xi}$) superposition of transient plane-waves (see Fig. 2). Their propagation properties follow from the delay term $v^{-1}(\boldsymbol{\xi}\cdot\mathbf{x}+\zeta z)$: For $|\boldsymbol{\xi}|<1$, they propagate in a direction $\boldsymbol{\kappa}$, whereas for $|\boldsymbol{\xi}|>1$, where $\zeta=i|\zeta|$ (see (4)), they decay as z increases (recall from (5) that an analytic signal decays monotonically as the imaginary part of its argument becomes more negative). Finally, for $z=0$, Eq. (12) is an inverse Radon transform of (11).

II.2.3. Real signals representation of the time-dependent plane-wave spectrum

The analytic signal representation in (11)–(12) incorporates both the propagating and the evanescent spectra in the same analytic framework. The real field is then obtained from the real part of (12). It might be useful, however, to express (11)–(12) directly in terms of

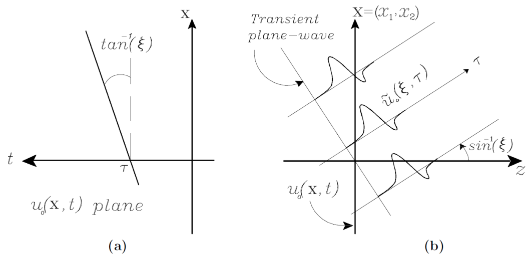

Figure 2. Transient plane-wave spectrum; **(a)** The transient plane-wave transform (the slant stack transform – SST) of the initial field $u_o(\mathbf{x}, t)$, **(b)** A transient plane-wave.

the *real* data $u_o(\mathbf{x}, t)$. Expressing u as the sum of the propagating and evanescent spectra, $u_P + u_E$ respectively, one immediately finds from (11)–(12), that

$$u_P(\mathbf{r}, t) = -(2\pi v)^{-2} \int_{|\boldsymbol{\xi}|<1} d^2\xi\, \partial_t^2 \widetilde{u}_o[\boldsymbol{\xi}, t - v^{-1}(\boldsymbol{\xi} \cdot \mathbf{x} + \zeta z)] \tag{13}$$

where $\widetilde{u}_o$ is the *real* transient plane-wave spectrum as obtained from u_o via the SST (see (11))

$$\widetilde{u}_o(\boldsymbol{\xi}, \tau) = \int d^2x\, u_o(\mathbf{x}, \tau + v^{-1}\boldsymbol{\xi} \cdot \mathbf{x}). \tag{14}$$

The evanescent spectrum contribution in (12) is given by

$$u_E(\mathbf{r}, t) = -(2\pi v)^{-2}\, \mathrm{Re} \int_{|\boldsymbol{\xi}|>1} d^2\xi\, \partial_t^2\, \overset{+}{\widetilde{u}}_o[\boldsymbol{\xi}, t - v^{-1}(\boldsymbol{\xi} \cdot \mathbf{x} + \zeta z)]. \tag{15}$$

This expression requires the calculation of $\overset{+}{\widetilde{u}}_o(\boldsymbol{\xi}, \tau)$ for complex τ: $\tau = t - v^{-1}(\boldsymbol{\xi} \cdot \mathbf{x} + i|\zeta|z)$. This can be done by transforming the data to the frequency domain, extracting the plane-wave spectrum via (2) for each ω and finally transforming for each $\boldsymbol{\xi}$ to complex τ via (9). Alternatively, this calculation may be performed directly from the time-dependent data using (6), giving

$$\overset{+}{\widetilde{u}}_o(\boldsymbol{\xi}, \tau) = \frac{1}{\pi i} \int d^2x \int dt'\, \frac{u_o(\mathbf{x}, t' + v^{-1}\boldsymbol{\xi} \cdot \mathbf{x})}{\tau - t'}, \quad \mathrm{Im}\tau < 0. \tag{16}$$

II.3. Discussion on spectral localization

The plane-wave integrals in (3) or (12) are spectrally distributed. For high frequency signals, however, dominant contributions are generated

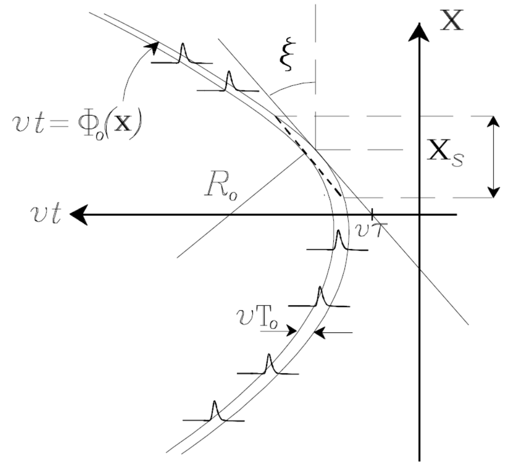

Figure 3. Asymptotic evaluation of the slant stack transform: The local radiation direction at a given $\mathbf{x}$ is determine by local matching of a pulsed plane-wave to the source distribution. For a given $\boldsymbol{\xi}$ this defines the stationary delay point $\mathbf{x}_s(\boldsymbol{\xi})$ of (18) that generates the dominant spectral contribution. The figure also provides the geometrical interpretation for the values of τ as obtained via the Legendre transform (19). The figure also depicts the asymptotic contributing zone (20) about the stationary point.

by localized regions in the source domain that emphasizes radiation in a given direction.

We assume that the source distribution has the short-pulse form (Fig. 3)

$$u_o(\mathbf{x}, t) = A_o[\mathbf{x}, t - v^{-1}\Phi_o(\mathbf{x})] \tag{17}$$

where $A_o(\mathbf{x}, t)$ is a short temporal pulse and $v^{-1}\Phi_o(\mathbf{x})$ is a delay function, both with slow spatial $\mathbf{x}$ variation (i.e., $|\partial_j A_o|$ and $|\partial_j \Phi_o|$ are much smaller than $v^{-1}\partial_t A_o$). It is then found that the dominant contribution to the plane-wave spectrum $\widetilde{u}_o(\boldsymbol{\xi}, \tau)$ in (11) comes from the region of the *stationary delay point* $\mathbf{x}_s(\boldsymbol{\xi})$, defined by

$$\nabla\Phi_o(\mathbf{x}) = \boldsymbol{\xi}, \quad \text{at} \quad \mathbf{x}_s(\boldsymbol{\xi}). \tag{18}$$

For a given $\mathbf{x}$, this condition defines the local radiation direction if a pulsed plane-wave is locally matched to the source distribution (see Fig. 3). In view of (14), $\widetilde{u}_o(\boldsymbol{\xi}, \tau)$ is concentrated about $\tau(\boldsymbol{\xi})$ as given by the Legendre transform [9]

$$\tau(\boldsymbol{\xi}) = v^{-1}[\Phi_o[\mathbf{x}_s(\boldsymbol{\xi})] - \boldsymbol{\xi} \cdot \mathbf{x}_s(\boldsymbol{\xi})]. \tag{19}$$

Its geometrical interpretation is schematized in Fig. 3. An illustrative numerical example will be considered in Sec. V.2.

The asymptotic localization above is valid only if the contributing zone around the stationary point is small with respect to the transverse variations of the field. As now follows from the local geometry in Fig. 3, if the pulse length of the data vT_o is much smaller than R_o (the local radius of curvature of the wavefront in the data plane $(\mathbf{x}, vt)$) then the asymptotic contributing zone (ACZ) is given by

$$\mathrm{ACZ} \sim 2\sqrt{2vT_oR_o} \sim \sqrt{vT_o/\det \partial^2_{ij}\Phi_o}, \tag{20}$$

where we have also quantified $R_o \sim 1/\sqrt{\det \partial^2_{ij}\Phi_o}$.

Likewise, the transient plane-wave superposition (12) can be localized by the stationary delayed evaluation: For a given observation point $\mathbf{r}$, the main contribution comes from the spectral direction $\boldsymbol{\xi}$ corresponding to the ray that emanates from the point $\mathbf{x}_s(\boldsymbol{\xi})$ in the $z = 0$ plane and passes through $\mathbf{r}$.

We shall not go through the compete asymptotic manipulations here as our goal is not to derive analytic ray-type local approximations. Instead in the next section we shall show how the phase-space representations yield spectral representations that are a priori localized about the ray skeleton define by (18)–(19).

III. LOCAL SPECTRA: PHASE-SPACE REPRESENTATION

III.1. Frequency-domain: Beam summation

III.1.1. Local spectrum of the data

We introduce the function $\widehat{U}_o$ as a windowed transform of the initial field

$$\widehat{U}_o(\bar{\mathbf{x}}, \bar{\boldsymbol{\xi}}) = \int d^2x\, \widehat{u}_o(\mathbf{x})\widehat{w}^*(\mathbf{x} - \bar{\mathbf{x}})\, e^{-ik\bar{\boldsymbol{\xi}}\cdot\mathbf{x}} \tag{21}$$

where $\widehat{w}(\mathbf{x})$ represents a spatial window function and the asterisk denotes a complex conjugate. Assuming $\hat{w}(\mathbf{x})$ to be localized around $\mathbf{x} = (0, 0)$, one may interpret $\widehat{U}_o$ as the *local spectral distribution* of $\widehat{u}_o$ in the vicinity of $\bar{\mathbf{x}}$. We shall therefore refer to $(\bar{\mathbf{x}}, \bar{\boldsymbol{\xi}})$ as phase-space coordinates, and adopt the notation $\mathbf{X} = (\bar{\mathbf{x}}, \bar{\boldsymbol{\xi}})$. Eq. (21) may now be written in the abbreviated form

$$\widehat{U}_o(\mathbf{X}) = \int d^2x\, \widehat{u}_o(\mathbf{x})\, \widehat{W}^*(\mathbf{x}; \mathbf{X}) \tag{22}$$

with the kernel

$$\widehat{W}(\mathbf{x};\mathbf{X}) = \widehat{w}(\mathbf{x}-\bar{\mathbf{x}})e^{ik\bar{\boldsymbol{\xi}}\cdot\mathbf{x}}. \tag{23}$$

Alternatively, the local spectrum $\widehat{U}_o$ can be evaluated from the plane-wave spectrum

$$\widehat{U}_o(\mathbf{X}) = (k/2\pi)^2 \int d^2\xi\ \widetilde{\widehat{u}}_o(\boldsymbol{\xi})\ \widetilde{\widehat{W}}^*(\boldsymbol{\xi};\mathbf{X}) \tag{24}$$

where $\widetilde{\widehat{W}}(\boldsymbol{\xi};\mathbf{X}) = \widetilde{\widehat{w}}(\boldsymbol{\xi}-\bar{\boldsymbol{\xi}})e^{-ik(\boldsymbol{\xi}-\bar{\boldsymbol{\xi}})\cdot\bar{\mathbf{x}}}$ with $\widetilde{\widehat{W}}$ and $\widetilde{\widehat{w}}$ being the spatial spectra (2) of $\widehat{W}$ and $\widehat{w}$, respectively. Thus, assuming also that $\widetilde{\widehat{w}}(\boldsymbol{\xi})$ is localized around $\boldsymbol{\xi}=(0,0)$, $\widehat{U}_o$ may also be considered as the local field corresponding to a sample of $\widetilde{\widehat{u}}_o$ around $\bar{\boldsymbol{\xi}}$.

The degree of spatial and spectral localization achieved can be quantified in terms of the spatial and spectral RMS widths of the window, defined, respectively, by

$$\Delta_x = \frac{1}{\widehat{N}}\left[\int d^2x|\mathbf{x}|^2\ |\widehat{w}(\mathbf{x})|^2\right]^{1/2}, \Delta_\xi = \frac{k}{\widehat{N}2\pi}\left[\int d^2\xi|\boldsymbol{\xi}|^2\ |\widetilde{\widehat{w}}(\boldsymbol{\xi})|^2\right]^{1/2} \tag{25 a, b}$$

where $\Delta_x\Delta_\xi \geq 1/k$ according to the uncertainty principle, and

$$\widehat{N} = \left[\int d^2x|\hat{w}(\mathbf{x})|^2\right]^{1/2} = (k/2\pi)\left[\int d^2\xi|\widetilde{\widehat{w}}(\boldsymbol{\xi})|^2\right]^{1/2} \tag{26}$$

is the $\mathcal{L}^2_{\mathbf{x}}$ norm of $\widehat{w}$.

By a straightforward extension of the 2D representation [20, 32], the inverse phase-space transform may be written formally as

$$\widehat{u}_o(\mathbf{x}) = (k/2\pi)^2\widehat{N}^{-2}\int d^4\bar{X}\ \widehat{U}_o(\mathbf{X})\ \widehat{W}(\mathbf{x};\mathbf{X}). \tag{27}$$

Note that this representation is not unique as there are many four variable kernels that can replace $\widehat{U}_o$ in (27) and still represent $\widehat{u}_o$. Of particular interest is the Gabor kernel [18–20, 23, 32]. However, the function $\widehat{U}_o$ of (21) yields the minimum energy representation [32].

III.1.2. The radiating field

The phase-space superposition (27) of the initial field can be propagated into the region $z>0$, giving

$$\widehat{u}(\mathbf{r}) = (k/2\pi)^2\widehat{N}^{-2}\int d^4\bar{X}\ \widehat{U}_o(\mathbf{X})\widehat{B}(\mathbf{r};\mathbf{X}) \tag{28}$$

where the phase-space propagator $\widehat{B}$ is the field radiated by each window element $\widehat{W}(\mathbf{x};\mathbf{X})$. $\widehat{B}$ can be expressed by several alternative ways (e.g. by Green's functions or plane-wave representations). In the present context it is convenient to express it by the plane-wave representation (3), i.e.

$$\widehat{B}(\mathbf{r};\mathbf{X}) = (k/2\pi)^2 \int d^2\xi \, \widetilde{\widehat{W}}(\boldsymbol{\xi};\mathbf{X}) \, e^{ik(\boldsymbol{\xi}\cdot\mathbf{x}+\zeta z)}. \tag{29}$$

If $\widehat{w}$ is wide on a wavelength scale then the spatial and spectral distributions of $\widehat{W}$ are localized around $\mathbf{x} = \bar{\mathbf{x}}$ and $\boldsymbol{\xi} = \bar{\boldsymbol{\xi}}$, respectively. Consequently, $\widehat{B}$ behaves like a collimated beam whose axis emerges from the $z = 0$ plane at $\mathbf{x} = \bar{\mathbf{x}}$ with a direction

$$\bar{\boldsymbol{\kappa}} = (\bar{\boldsymbol{\xi}}, \bar{\zeta}), \quad \bar{\zeta} = \sqrt{1 - |\bar{\boldsymbol{\xi}}|^2} \tag{30}$$

where $|\bar{\boldsymbol{\xi}}|^2 = \bar{\boldsymbol{\xi}} \cdot \bar{\boldsymbol{\xi}}$. Propagating beams occur only for $|\bar{\boldsymbol{\xi}}| < 1$ or more precisely, for $|\bar{\boldsymbol{\xi}}| < (1 - \Delta_\xi)$ where Δ_ξ is defined in (25b). For $|\bar{\boldsymbol{\xi}}| > 1$, $\widehat{B}$ decays exponentially with z.

The representation in (28) describes the radiated field as a continuous superposition of shifted and tilted beams, centered at and directed along $\bar{\mathbf{x}}$ and $\bar{\boldsymbol{\xi}}$, respectively (see Fig. 1). The phase-space function $\widehat{U}_o$ defines the excitation strengths of these beams via local matching to the aperture field $\widehat{u}_o(\mathbf{x})$.

III.1.3. Spectral localization

An important feature of the representation above is the a priori localization around well defined regions in the $\mathbf{X}$ domain. This localization is affected by both $\widehat{U}_o$ and $\widehat{B}$ in (28). Since each beam has a finite spatial and spectral widths in the aperture plane, it senses via (21) the local radiation properties of $\widehat{u}_o(\mathbf{x})$ at $\bar{\mathbf{x}}$. Accordingly $\widehat{U}_o$ favors *a priori* the beams that emanate from $\bar{\mathbf{x}}$ along the *local preferred direction* (see Fig. 1). If for example, $\widehat{u}_o(\mathbf{x})$ has the high frequency form (c.f. (17))

$$\widehat{u}_o(\mathbf{x}) = \widehat{A}_o(\mathbf{x}) e^{ik\Phi_o(\mathbf{x})} \tag{31}$$

then $\widehat{U}_o$ and thereby the integration domain in (28) are limited to the vicinity of the *radiation direction* constraint

$$\bar{\boldsymbol{\xi}} = \nabla\Phi_o(\bar{\mathbf{x}}). \tag{32}$$

This constraint defines the local direction of radiation (see (18)). In many situations, however, the form of the constraint may be more complicated. For example, if $\widehat{u}_o$ represents the scattered field data due to several localized scatterers, then it consists of several additive terms like (31) and the integration domain in (28) involves several constraints like (32), with possible overlap.

The effective domain of integration in (28) is limited further because only those beams that pass near $\mathbf{r}$ actually contribute. For a given $\mathbf{r}$ this localizes the contributions in (28) to the vicinity of a hyper-plane in the $\mathbf{X}$-domain, defined by

$$(\mathbf{x}-\bar{\mathbf{x}})/\bar{R}=\bar{\boldsymbol{\xi}}, \quad \bar{R}\equiv\sqrt{|\mathbf{x}-\bar{\mathbf{x}}|^2+z^2}. \tag{33}$$

This *observation constraint* defines the phase-space beams that pass through $\mathbf{r}$.

Thus, unlike the plane-wave superposition, the phase-space beam representation is localized *a priori* in the $\mathbf{X}$-domain about the skeleton as schematized in Fig. 1. It emphasizes only those beam that emanate along the local radiation direction (32) and also pass near the observation point as defined in (33).

III.2. Time-domain: Pulsed-beam summation

III.2.1. Local spectrum of the data

The time-dependent local spectral distribution of the initial field is defined as an inverse Fourier transform of the $\widehat{U}_o(\mathbf{X})$ in (21)

$$U_o(\mathbf{Y})=\frac{1}{2\pi}\int_{-\infty}^{\infty}d\omega\;\widehat{U}_o(\mathbf{X};\omega)\;e^{-i\omega(\bar{t}-v^{-1}\bar{\boldsymbol{\xi}}\cdot\bar{\mathbf{x}})}, \tag{34}$$

where $\bar{t}$ denotes the phase-space time variable in the five dimensional phase-space $\mathbf{Y}\equiv(\bar{\mathbf{x}},\bar{\boldsymbol{\xi}},\bar{t})$. The time shift,$v^{-1}\bar{\boldsymbol{\xi}}\cdot\bar{\mathbf{x}}$, in the exponent of (34) has been introduced for a convenient interpretation of the results (see discussions following (39) and (46)).

In order to express $U_o(\mathbf{Y})$ directly in terms of the time-dependent data we apply (34) to (22), to obtain

$$U_o(\mathbf{Y})=\frac{1}{2\pi}\int_{-\infty}^{\infty}d\omega\int d^2x\;\widehat{u}_o(\mathbf{x};\omega)\widehat{W}^*(\mathbf{x};\mathbf{X};\omega)\;e^{-i\omega(\bar{t}-v^{-1}\bar{\boldsymbol{\xi}}\cdot\bar{\mathbf{x}})}. \tag{35}$$

Inverting the order of integrations and using the convolution theorem we obtain

$$U_o(\mathbf{Y})=\int d^2x\int dt\;u_o(\mathbf{x},t)\;W(\mathbf{x},t;\mathbf{Y}) \tag{36}$$

where the phase-space kernel $W(\mathbf{x},t;\mathbf{Y})$ is related to $\widehat{W}(\mathbf{x};\mathbf{X})$ of (23) via

$$W(\mathbf{x},t;\mathbf{Y}) = \frac{1}{2\pi}\int_{-\infty}^{\infty} d\omega\, \widehat{W}^*(\mathbf{x};\mathbf{X};\omega)\, e^{-i\omega(\bar{t}-t-v^{-1}\bar{\boldsymbol{\xi}}\cdot\bar{\mathbf{x}})} \tag{37}$$

Substituting $\widehat{W}(\mathbf{x};\mathbf{X}) = \widehat{w}(\mathbf{x}-\bar{\mathbf{x}})e^{ik\bar{\boldsymbol{\xi}}\cdot\mathbf{x}}$ (23) and noting that $w(\mathbf{x},t)$ is real so that $\widehat{w}^*(\omega) = \widehat{w}(-\omega)$ we obtain

$$W(\mathbf{x},t;\mathbf{Y}) = \frac{1}{2\pi}\int_{-\infty}^{\infty} d\omega\, \widehat{W}(\mathbf{x};\mathbf{X};\omega)\, e^{-i\omega(t-\bar{t}+v^{-1}\bar{\boldsymbol{\xi}}\cdot\bar{\mathbf{x}})} \tag{38}$$

and finally from (23)

$$W(\mathbf{x},t;\mathbf{Y}) = w[\mathbf{x}-\bar{\mathbf{x}}, t-\bar{t}-v^{-1}\bar{\boldsymbol{\xi}}\cdot(\mathbf{x}-\bar{\mathbf{x}})] \tag{39}$$

where the window functions $w(\mathbf{x},t)$ is the TD counterpart of the FD window function $\widehat{w}(\mathbf{x})$ via (1 b). Typical parameters for the space-time support of this window function will be considered in Sec. IV.2.

It is assumed that $w(\mathbf{x},t)$ is localized about the origin, hence the phase-space window W of (39) is localized about $\mathbf{x} = \bar{\mathbf{x}}$ and $t = \bar{t} + v^{-1}\bar{\boldsymbol{\xi}}\cdot(\mathbf{x}-\bar{\mathbf{x}})$. Thus (36) is readily identified as a *windowed Radon transform* localized about $(\mathbf{x},t) = (\bar{\mathbf{x}},\bar{t})$ with the spectral tilt $\bar{\boldsymbol{\xi}}$ (see Fig. 4a). This interpretation identifies U_o as the local time-dependent spectrum of u_o (compare Fig. 2). For proper numerical implementation of the local transform in (36) we shall demand that w is in $\mathcal{L}^1_{(\mathbf{x},t)}$, namely

$$\int d^2x \int dt\, |w(\mathbf{x},t)| = \text{finite.} \tag{40}$$

The inversion formula corresponding to (36) is found by transforming (27) into the TD and following essentially the same analytic procedure. The result is

$$u_o(\mathbf{x},t) = -(2\pi v)^{-2}\int d^5Y\, U_o(\mathbf{Y})W_N(\mathbf{x},t;\mathbf{Y}) \tag{41}$$

where

$$W_N(\mathbf{x},t;\mathbf{Y}) = N^\dagger(t)\otimes W(\mathbf{x},t;\mathbf{Y}) \tag{42}$$

and

$$N^\dagger(t) = \frac{1}{2\pi}\int d\omega\, (-i\omega)^2\widehat{N}^{-2}(\omega)\, e^{-i\omega t}. \tag{43}$$

Note that $\widehat{N}$ may tend to zero as $\omega\to\infty$, in which case the integral in (43) does not converge. Nevertheless, in the case of band limited signals the integration domain in (43) may be limited to the maximum frequency of the excitation so that (43) is well define (see also discussion preceding (69)).

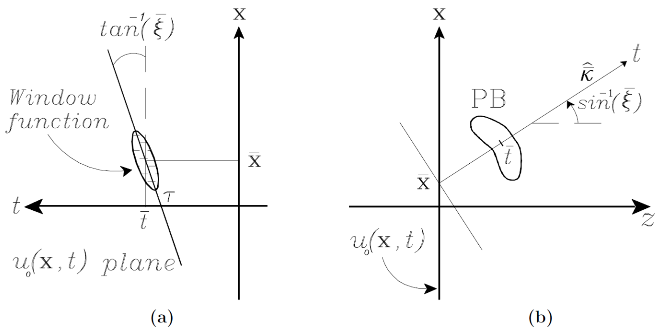

Figure 4. Local (Pulsed-beam) spectrum; **(a)** The local Radon transforms of the initial field $u_o(\mathbf{x}, t)$, **(b)** A radiating pulsed-beam.

III.2.2. The radiating field

Eq. (41) can be propagated to $z > 0$, giving

$$u(\mathbf{r}, t) = -(2\pi v)^{-2} \int d^5Y\ U_o(\mathbf{Y}) B(\mathbf{r}, t; \mathbf{Y}) \tag{44}$$

where the propagators $B(\mathbf{r}, t; \mathbf{Y})$ describes the radiation into the half space $z > 0$ due to field distribution $W_N(\mathbf{x}, t; \mathbf{Y})$ in the $z = 0$ plane. In view of (28) and (34) they are related to the FD beam propagators $\widehat{B}(\mathbf{r}; \mathbf{X})$ of (29) via

$$B(\mathbf{r}, t; \mathbf{Y}) = \frac{1}{2\pi} \int_{-\infty}^{\infty} d\omega\ (-i\omega)^2 \widehat{N}^{-2}(\omega) \widehat{B}(\mathbf{r}; \mathbf{X}; \omega)\ e^{-i\omega[t - \bar{t} + v^{-1} \bar{\boldsymbol{\xi}} \cdot \bar{\mathbf{x}}]}. \tag{45}$$

$B(\mathbf{r}, t; \mathbf{Y})$ may also be calculated directly from field distribution $W(\mathbf{x}, t; \mathbf{Y})$ in the $z = 0$ plane via several alternative TD formulations (e.g. Kirchhoff integral). Following (29) we shall represent it here by a transient plane-wave integral. Since B may contains an evanescent spectrum, in addition to the propagating spectrum, we shall utilize the analytic signal representation (12). Thus $B(\mathbf{r}, t; \mathbf{Y}) = \mathrm{Re}\ \overset{+}{B}(\mathbf{r}, t; \mathbf{Y})$ with

$$\overset{+}{B}(\mathbf{r}, t; \mathbf{Y}) = -(2\pi v)^{-2} \int d^2\xi\ \overset{+}{\widetilde{W}}_N(\boldsymbol{\xi}, t - v^{-1}(\boldsymbol{\xi} \cdot \mathbf{x} + \zeta z); \mathbf{Y}) \tag{46}$$

where $\overset{+}{\widetilde{W}}_N(\boldsymbol{\xi}, \tau; \mathbf{Y})$ is the analytic transient plane-wave spectrum (11) of $W_N(\mathbf{x}, t; \mathbf{Y})$. In view of (39) it is given by $\overset{+}{\widetilde{W}}_N(\boldsymbol{\xi}, \tau; \mathbf{Y}) = N^\dagger(t) \otimes \overset{+}{\widetilde{w}}$

$(\boldsymbol{\xi}-\bar{\boldsymbol{\xi}}, \tau-\bar{t}+v^{-1}\boldsymbol{\xi}\cdot\bar{\mathbf{x}})$ where $\overset{+}{\tilde{w}}(\boldsymbol{\xi},\tau)$ denotes the analytic plane-wave spectrum (11) of $\overset{+}{w}(\mathbf{x},t)$.

Since from (39) $\overset{+}{W}$ is localized about $(\mathbf{x},\boldsymbol{\xi},t) = (\bar{\mathbf{x}},\bar{\boldsymbol{\xi}},\bar{t}) = \mathbf{Y}$, $\overset{+}{B}$ describes a space-time wavepacket (pulsed-beam - PB) that emerges from the $z=0$ plane at $(\mathbf{x},t) = (\bar{\mathbf{x}},\bar{t})$ in the direction $\bar{\boldsymbol{\kappa}}$ of (30) (see Fig 4a). Closed form expressions for $\overset{+}{B}$ will be considered in Sec. IV.2.

III.2.3. Spectral localization

The representation in (44) describes the field as a continuous spectrum of shifted, tilted and delayed PB (Fig. 1). The PB amplitude is described by the local spectral function U_o that matches this spectrum to the given aperture distribution. If the aperture is smooth enough, then U_o senses the local radiation properties of the aperture around $\bar{\mathbf{x}}$ and therefore excites only those PB propagators that match those properties (Fig. 4). The integral representation (44) is therefore localized *a priori* in the $\mathbf{Y}$ domain (without recourse to asymptotic analysis).

Assuming for example that u_o is a short-pulse distribution of the form (17), then U_o enhances PB whose phase-space coordinates $\mathbf{Y}$ are in the vicinity of the *radiation constraint* (see (32) and Fig. 1)

$$\bar{\boldsymbol{\xi}} = \nabla\Phi_o(\bar{\mathbf{x}}), \quad \bar{t} = v^{-1}\Phi_o(\bar{\mathbf{x}}) \tag{47}$$

This limits the effective domain of integration in (44) to phase-space regions adjacent to that constraint. The integration domain is limited further due to the fact that the PB propagators B are confined in space-time, so that non-negligible contributions are obtained only from PBs that pass near the observation point. For a given $(\mathbf{r},t)$ this constraints the relevant phase-space coordinates to the vicinity of the *observation constraint* (see (33))

$$(\mathbf{x}-\bar{\mathbf{x}})/\bar{R} = \bar{\boldsymbol{\xi}} \;\; , \;\; \bar{t} = t - \bar{R}/v. \tag{48}$$

Thus, the actual integration domain in (44) is confined, *a priori* to compact domains around the intersection of the constraints in (47) and (48). The degree of localization depends on the choice of the proper window function w which minimizes the phase-space support of both U_o and B for a given class of initial distributions, and for a given observations range. This subject will be addressed next by considering special window functions.

IV. GAUSSIAN WINDOWS

Gaussian windows have several important properties: (a) they maximize the phase-space localization implied by the uncertainty principle; (b) they generate tractable beam propagators which are related to the conventional Gaussian beams; (c) they are well suited to performing analytic approximations; (d) they furnish convenient basis functions for time-dependent representations (see Sec. IV.2).

IV.1. Time-harmonic Gaussian window

IV.1.1. Properties of the window function

A 2D Gaussian window has the general form

$$\widehat{w}(\mathbf{x}) = e^{-\frac{1}{2}k\,\mathbf{x}\cdot\boldsymbol{\beta}^{-1}\cdot\mathbf{x}} \tag{49}$$

where $\boldsymbol{\beta}^{-1}$ is symmetrical complex matrix so that $\mathbf{x}\cdot\boldsymbol{\beta}^{-1}\cdot\mathbf{x}$ is a quadratic form. For convergence at large $\mathbf{x}$, $\mathrm{Re}\boldsymbol{\beta}^{-1}$ should be positive definite for $\omega > 0$. Henceforth we shall only consider rotationally symmetric windows where $\boldsymbol{\beta} = \beta\mathbf{I}$ with $\mathbf{I}$ being the identity matrix and $\beta = \beta_r + i\beta_i$ with $\beta_r > 0$ for $\omega > 0$. These spatial and spectral window functions have the form

$$\widehat{w}(\mathbf{x}) = e^{-\frac{1}{2}k\,|\mathbf{x}|^2/\beta}, \quad \widehat{\widetilde{w}}(\boldsymbol{\xi}) = (2\pi\beta/k)e^{-\frac{1}{2}k\,\beta|\boldsymbol{\xi}|^2} \tag{50}$$

with the norm and width (see (25)–(26))

$$\widehat{N}^2 = (\pi/k)|\beta|^2/\beta_r, \quad \Delta_x = |\beta|/\sqrt{\beta_r k} = \Delta_\xi|\beta|. \tag{51}$$

Note the uncertainty principle $\Delta_x\Delta_\xi = |\beta|/\beta_r k \geq 1/k$ with an equality for $\beta = \beta_r$. Note also that we have kept the frequency parameter k explicit in the exponent of (50). The resulting beam propagator will have *frequency independent* collimation distance but *frequency dependent* widths (see (57), (58)). This will have a major effect on the shape of the TD window and propagators (see Sec. IV.2).

IV.1.2. Properties of the propagators

The phase-space propagators $\widehat{B}(\mathbf{r};\mathbf{X})$ are calculated by substituting (50) in (29). For large $k\beta_r$ the integral can be evaluated asymptotically as detailed in Appx. VI. The result is listed below. We utilize the beam axis coordinates (x_{b_1}, x_{b_2}, z_b) defined, for a given phase-space point $\mathbf{X}$,

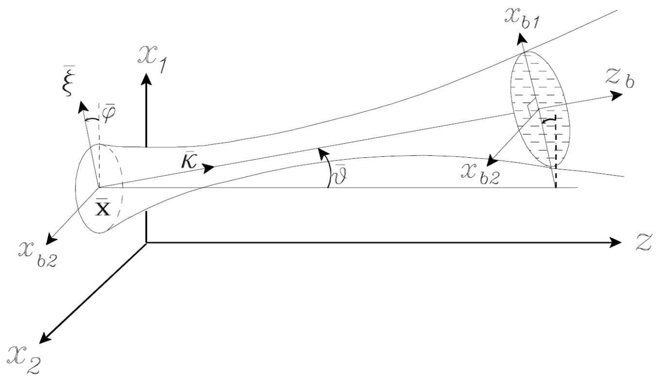

Figure 5. The beam field in the configuration space. The beam emerges from $\bar{\mathbf{x}}$ along the $\bar{\boldsymbol{\kappa}}$ direction identified by the spherical angles $(\bar{\vartheta}, \bar{\varphi})$. The z_b axis coincides with the beam axis while the transverse beam coordinates (x_{b_1}, x_{b_2}), defined in (52), are rotated such that x_{b_1} lies in the plane $(\bar{\boldsymbol{\xi}}, \bar{\boldsymbol{\kappa}})$. Consequently x_{b_2} is parallel the z-plane.

by the transformation

$$\begin{bmatrix} x_{b_1} \\ x_{b_2} \\ z_b \end{bmatrix} = \begin{bmatrix} \cos\bar{\vartheta}\cos\bar{\varphi} & \cos\bar{\vartheta}\sin\bar{\varphi} & -\sin\bar{\vartheta} \\ -\sin\bar{\varphi} & \cos\bar{\varphi} & 0 \\ \sin\bar{\vartheta}\cos\bar{\varphi} & \sin\bar{\vartheta}\sin\bar{\varphi} & \cos\bar{\vartheta} \end{bmatrix} \begin{bmatrix} x_1 - \bar{x}_1 \\ x_2 - \bar{x}_2 \\ z \end{bmatrix} \tag{52}$$

where $(\bar{\vartheta}, \bar{\varphi})$ are the spherical angles that define the beam direction $\bar{\boldsymbol{\kappa}} = (\bar{\boldsymbol{\xi}}, \bar{\zeta})$ (Fig. 5), i.e.

$$\cos\bar{\vartheta} = \bar{\zeta}, \quad \cos\bar{\varphi} = \bar{\xi}_1/|\bar{\boldsymbol{\xi}}|, \quad \sin\bar{\varphi} = \bar{\xi}_2/|\bar{\boldsymbol{\xi}}|. \tag{53}$$

Thus, the z_b axis coincides with the beam axis while the transverse coordinates $\mathbf{x}_b = (x_{b_2}, x_{b_1})$ are rotated such that x_{b_1} lies in the plane $(\bar{\boldsymbol{\xi}}, \bar{\boldsymbol{\kappa}})$ (see Fig. 5). Accordingly, the linear phase $\bar{\boldsymbol{\xi}} \cdot \mathbf{x}$ implied by the window function in the $z = 0$ plane (see (21)) is operative in the x_{b_1} direction *but not* in the x_{b_2} direction. Utilizing the beam coordinates we obtain by saddle point integration (see Appx. VI)

$$\widehat{B}(\mathbf{r}; \mathbf{X}) \sim \widehat{B}_s = \sqrt{\frac{\det\ \mathbf{Q}(z)}{\det\ \mathbf{Q}(0)}}\ e^{ik\,(\bar{\mathbf{x}}\cdot\bar{\boldsymbol{\xi}} + z_b + \frac{1}{2}\mathbf{x}_b\cdot\mathbf{Q}\cdot\mathbf{x}_b)} \tag{54}$$

where

$$\mathbf{Q} = \begin{bmatrix} (z\bar{\zeta}^{-1} - i\beta\bar{\zeta}^2)^{-1} & 0 \\ 0 & (z\bar{\zeta}^{-1} - i\beta)^{-1} \end{bmatrix}. \tag{55}$$

In view of (55), the quadratic form $\mathbf{x}_b \cdot \mathbf{Q} \cdot \mathbf{x}_b$ in (54) is given by $x_{b_1}^2 Q_{11} + x_{b_2}^2 Q_{22}$.

The properties of $\widehat{B}$ either as a configuration-space object, where $\mathbf{X}$ is kept constant and $\widehat{B}$ is regarded as a function of $\mathbf{r}$, or as a phase-space object, where $\mathbf{r}$ is kept constant and $\mathbf{X}$ is varied, are discussed next. Regarded as a function of $\mathbf{r}$, $\widehat{B}_s$ of (54) has essentially the form of a Gaussian beam (GB), propagating along the beam axis z_b. However, in the conventional GB the elements of $\mathbf{Q}$ depend only on the location along the beam axis (i.e. on z_b; see (56)–(59)), whereas in (55) they depend on $z = \bar{\zeta} z_b - |\bar{\boldsymbol{\xi}}| x_{b_1}$. This difference is due to the fact that in the conventional GB, the Gaussian initial conditions are given on a plane normal to the beam axis, whereas here they are defined on a plane of constant z which is generally inclined with respect to the beam axis. It is important, therefore, to observe that $\widehat{B}_s$ in (54) conforms smoothly to the specified Gaussian distribution $\widehat{W}(\mathbf{x};\mathbf{X})$ in $z = 0$ plane.

IV.1.3. Paraxial form

For large z_b or near the beam axis, $\widehat{B}_s$ of (54) changes smoothly into a conventional GB. It is described by (54)–(55) wherein we substitute, from (52), $z\bar{\zeta}^{-1} = z_b - x_{b_1} \tan\bar{\vartheta} \simeq z_b$. Under this paraxial substitution, we express the elements of $\mathbf{Q}$ in (55) in the form

$$(z\bar{\zeta}^{-1} - i\beta\bar{\zeta}^2)^{-1} \to (z_b - i\beta\bar{\zeta}^2)^{-1} = (z_b - Z_1 - iF_1)^{-1} = 1/R_1 + i/kD_1^2 \tag{56 a}$$

$$(z\bar{\zeta}^{-1} - i\beta)^{-1} \to (z_b - i\beta)^{-1} = (z_b - Z_2 - iF_2)^{-1} = 1/R_2 + i/kD_2^2 \tag{56 b}$$

where the parameters

$$Z_1 = -\beta_i\bar{\zeta}^2, \quad F_1 = \beta_r\bar{\zeta}^2, \quad Z_2 = -\beta_i, \quad F_2 = \beta_r \tag{57}$$

will be interpreted below. Furthermore, for $j = 1, 2$ we obtain from (56)

$$D_j = \sqrt{F_j/k}\sqrt{1 + (z_b - Z_j)^2/F_j^2} \tag{58}$$

$$R_j = (z_b - Z_j) + F_j^2/(z_b - Z_j). \tag{59}$$

By substituting (56 a,b) into (54) one readily identifies D_j as the *beam width* in the (z, x_{b_j}) plane, while R_j is the *phase front radius of curvature*. The resulting GB is therefore *astigmatic*; its *waist* in the (z, x_{b_j}) plane, is located at $z_b = Z_j$, while F_j is the corresponding *collimation length*. This astigmatism is caused by the beam tilt which reduces the effective initial beam width in the x_{b_1} direction.

Regarding $\widehat{B}$ as a function of $\mathbf{X}$ for a fixed $\mathbf{r}$ one finds from (54) that $\widehat{B}_s$ exhibits a Gaussian decay away from the constraint plane of (33). Keeping $\bar{\boldsymbol{\xi}}$ constant, one finds that the Gaussian widths as $\mathbf{X}$ is displaced from this constraint in the x_{b_1} and x_{b_2} directions are given by

$$\bar{D}_1 = D_1/\bar{\zeta}, \quad \bar{D}_2 = D_2. \tag{60}$$

This also determined, via (33), the Gaussian widths of the decay as $\mathbf{X}$ displaced in the ξ_1 and ξ_2 directions.

IV.2. Time-dependent Gaussian-δ window

IV.2.1. Properties of the window function

A convenient TD window is obtained by transforming the FD Gaussian window (50), with β being *frequency independent*. Note though that convergence of the window in (50) implies $\beta|_{\omega<0} = -\beta^*|_{\omega>0}$, so it is convenient to utilize the analytic signal representation (5). Thus, applying (5) to $\widehat{w}$ of (50) we obtain

$$w(\mathbf{x}, t) = \mathrm{Re}\, \overset{+}{w}(\mathbf{x}, t) = \mathrm{Re}\, \overset{+}{\delta}[t - v^{-1}\frac{i}{2}|\mathbf{x}|^2/\beta] \tag{61}$$

where $\overset{+}{\delta}$ is the analytic delta function

$$\overset{+}{\delta}(t) = \begin{cases} (\pi i t)^{-1}, & \mathrm{Im} t < 0 \\ \delta(t) + \mathcal{P}(\pi i t)^{-1}, & \mathrm{Im} t = 0 \end{cases} \tag{62}$$

with $\mathcal{P}$ indicating Cauchy's principal value. This window is localized around $(\mathbf{x}, t) = (0, 0)$. For $|\mathbf{x}| = 0$, it is impulsive at $t = 0$ and decays thereafter like t^{-1}. For $|\mathbf{x}| \neq 0$, the argument of the $\overset{+}{\delta}$ function in (61) has a negative imaginary part and thus the window has the form of a smooth Lorentzian pulse.

One may readily verify that the decay rate of the window in (61) is not fast enough in t and $\mathbf{x}$ and thus it is not in $\mathcal{L}^1_{(\mathbf{x},t)}$ (see (40)). In order to obtain a window in $\mathcal{L}^1_{(\mathbf{x},t)}$ we shall differentiate this window twice. Furthermore, as noted above, the window in (61) is impulsive for $\mathbf{x} = 0$. In a numerical processing, one may analytically extract the contribution of the δ-singularity in the local Radon transform integral (36). In general, however, it is convenient to use a smooth window. Such a window is obtained if an exponential decay $e^{-\omega T/2}$ is added to $\widehat{w}$ in (50), where the parameter $T > 0$ is chosen to satisfy

$$T \ll \omega_{max}^{-1} \tag{63}$$

with ω_{max} denoting the upper frequency in the data $u_o(\mathbf{x}, t)$. The reason for condition (63) will be discussed in connection with (69). Thus, applying (5) to $\widehat{w}(\mathbf{x}, \omega) = (-i\omega)^2 \, e^{-\frac{1}{2}k\,\beta^{-1}|\mathbf{x}|^2 - \frac{1}{2}\omega T}$ we obtains, instead of (61), the window function

$$w(\mathbf{x}, t) = \text{Re } \overset{+}{w}(\mathbf{x}, t) = \text{Re } \overset{+}{\delta}{}^{(2)}[t - \frac{i}{2}T - v^{-1}\frac{i}{2}|\mathbf{x}|^2/\beta]. \tag{64}$$

where from (62), $\overset{+}{\delta}{}^{(2)}(t) \equiv \overset{+}{\delta}{}''(t) = 2/\pi i t^3$.

To clarify the properties of this window we shall rewrite it in a standard form

$$w(\mathbf{x}, t) = \text{Re } \overset{+}{\delta}{}''[t - t_p - \frac{i}{2}T_p] = \partial_t^2 \, \frac{1}{\pi} \frac{T_p/2}{(t - t_p)^2 + (T_p/2)^2} \tag{65}$$

where

$$t_p(\mathbf{x}) = \frac{1}{2}\frac{\beta_i}{v|\beta|^2}|\mathbf{x}|^2, \qquad T_p(\mathbf{x}) = T + \frac{\beta_r}{v|\beta|^2}|\mathbf{x}|^2 \tag{66}$$

To parameterize the properties of this window we shall consider the expression in (65) without the second time-derivative. For a given $\mathbf{x}$ this expression peaks at $t = t_p(\mathbf{x})$ and its pulse-length and peak-value are given, respectively, by $T_p(\mathbf{x})$ and $2/\pi T_p(\mathbf{x})$. As $|\mathbf{x}|$ increases, T_p increases and thus w decays (see Fig. 6). The transverse half-amplitude diameter of the window, D, is therefore obtained by solving $T_p(\mathbf{x}) = 2T_p(0)$, giving

$$D = 2\sqrt{T|\beta|^2 v/\beta_r}. \tag{67}$$

Next we shall estimate the size of the integration domain around the window center needed in a numerical implementation with the local window transform (36). We shall consider the error in the $\mathcal{L}^1_{(\mathbf{x},t)}$ norm of the window in (64) when the integration domain is truncated, i.e.,

$$||w|| = \text{Re} \int_0^{\rho_{max}} \rho d\rho \int_{-t_{max}}^{t_{max}} dt \; |w(\rho, t)| \tag{68}$$

where $\rho = |\mathbf{x}|$. Evaluating this integral in close form for $\rho_{max} \to \infty$ and $t_{max} \to \infty$ we obtain $||w|| = 3\sqrt{3}\beta/\pi T$. When the integration domain is truncated as in (68), the norm may also be evaluated analytically. The resulting relative error, E, is depicted in Fig. 7. One can show that the error is proportional asymptotically to T/t_{max} and to $(D/2\rho_{max})^2$ where D is the transverse half-amplitude diameter of the window (67).

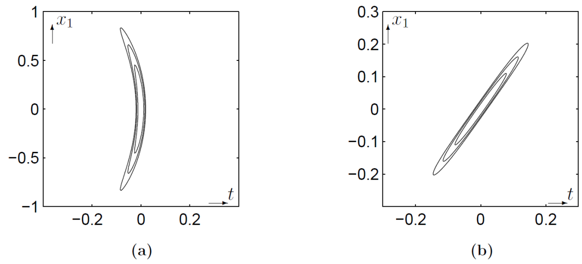

Figure 6. The Gaussian-δ window (64) in the (x_1, t) plane. The contour levels are at 3db, 6db and 9db of the peak. The window are depicted for $\bar{\mathbf{x}} = 0$, $\bar{t} = 0$, $T = 0.1$, $v = 1$ and for **(a)** $\bar{\boldsymbol{\xi}} = 0$ and $\beta = 1 - 4i$ (a slightly focusing window); **(b)** $\beta = 1$ and $\bar{\boldsymbol{\xi}} = (\sqrt{2}/2, 0)$ (the PB radiates in 45^o).

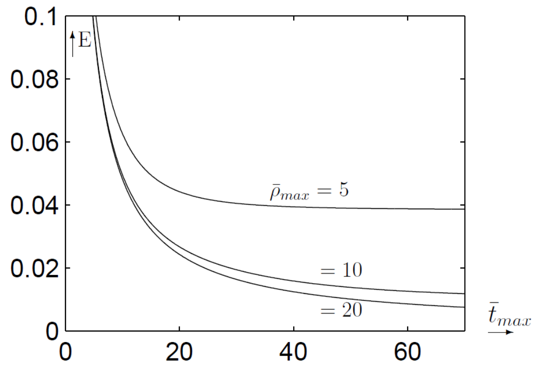

Figure 7. The relative error, E, in the norm $||w(\mathbf{x}, t)||$ for the Gaussian-δ window in (64) as a function of the normalized time and space truncation $\bar{t}_{max} = t_{max}/T$ and $\bar{\rho}_{max} = \rho_{max}/(D/2)$.

IV.2.2. Properties of the propagators

Next we shall calculate the beam propagators for the TD window in (65). For well collimated windows, closed form expressions for $\overset{+}{B}$ can be obtained via an asymptotic evaluation of the spectral integral (46) *directly* in the TD. For simplicity, however, we shall derive these expressions from the asymptotic FD beams $\widehat{B}_s$ in (54). Noting that the TD window in (64) corresponds to the FD window $\widehat{w}(\mathbf{x}, \omega) = (-i\omega)^2 \, e^{-\frac{1}{2}k\,\beta^{-1}|\mathbf{x}|^2 - \frac{1}{2}\omega T}$, we find that the corresponding FD propagators are given by $(-i\omega)^2 e^{-\frac{1}{2}\omega T}\widehat{B}_s$. Furthermore, using (51) we have for this FD window $\widehat{N}^2 = (-i\omega)^4 \frac{\pi}{k}\frac{|\beta|^2}{\beta_r} e^{-\omega T}$ so that (43) for $N^\dagger$ *does not* converge for real t. However, if T is chosen according to (63) then it has no effect over the entire frequency band of the data so that we may use $T = 0$ in the expression for $\widehat{N}^2$ (see also discussion in (43)). Substituting in (45), we obtain for the TD propagators $B(\mathbf{r}, t; \mathbf{Y}) = \mathrm{Re}\ \overset{+}{B}(\mathbf{r}, t; \mathbf{Y})$ where

$$\begin{aligned}\overset{+}{B}(\mathbf{r}, t; \mathbf{Y}) &\simeq \frac{1}{\pi}\int_0^\infty \frac{k\beta_r}{\pi|\beta|^2}\widehat{B}_s(\mathbf{r}; \mathbf{X}; \omega)\ e^{-i\omega[t-\bar{t}+v^{-1}\bar{\boldsymbol{\xi}}\cdot\bar{\mathbf{x}}]}\\ &= \frac{i\partial_t\beta_r}{\pi v|\beta|^2}\sqrt{\frac{\det \mathbf{Q}(z)}{\det\ \mathbf{Q}(0)}}\ \overset{+}{\delta}\,[t-\bar{t}-\frac{i}{2}T - v^{-1}(z_b + \frac{1}{2}\mathbf{x}_b\cdot\mathbf{Q}\cdot\mathbf{x}_b)].\end{aligned} \tag{69}$$

The last expression is written in terms of the beam coordinates (x_{b_1}, x_{b_2}, z_b) defined in (52) while $\mathbf{Q}$ is given by (55). This expression readily establishes B as a PB field that emanates from the point $\mathbf{x} = \bar{\mathbf{x}}$, in the $z = 0$ plane at a time $t = \bar{t}$, and propagates in the $\bar{\boldsymbol{\kappa}}$ direction along the z_b axis. The confinement along the propagation axis is described by the pulse shape $\overset{+}{\delta}\,(t - \bar{t} - v^{-1}z_b - \frac{i}{2}T)$, which implies that the wavepacket is centered about $z_b = v(t - \bar{t})$. The spatial confinement transverse to the beam axis is described by the quadratic form $-\frac{1}{2}v^{-1}\mathbf{x}_b\cdot\mathbf{Q}\cdot\mathbf{x}_b$: Noting from (55), with $\beta_r > 0$, that this term has a negative imaginary part that increases quadratically as the distance from the axis increases, it follows that $\overset{+}{B}$ decays away from the axis.

The PB is (69) has the form of an astigmatic PB field [13]. However, in a conventional PB, the elements of $\mathbf{Q}$ depend only on z_b, i.e., on the location *along* the beam axis, whereas here they depend on $z = \bar{\zeta}z_b - |\bar{\boldsymbol{\xi}}|x_{b_1}$. The reason for this has already been discussed after (55). It follows that expression (69) conforms smoothly with the initial field distribution $W_N(\mathbf{x}, t; \mathbf{Y})$ at the $z = 0$ plane.

For large z_b, on the other hand, we may replace in $\mathbf{Q}$: $z\bar{\zeta}^{-1} = z_b - x_{b_1}\tan\bar{\vartheta} \simeq z_b$, hence (69) changes gradually into a conventional PB. In this case, the space-time structure of $\overset{+}{B}$ may be characterized by rewriting the elements of $\mathbf{Q}$ in (55) in the form

$$(z_b - Z_j - iF_j)^{-1} \equiv 1/R_j + i/I_j \tag{70}$$

where for $j = 1$ or 2, $R_j(z_b)$ is given in (59) and (cf. (58))

$$I_j(z_b) = F_j(1 + (z_b - Z_j)^2/F_j^2). \tag{71}$$

Expression (69) for the PB field may therefore be written in a standard form

$$\overset{+}{B}(\mathbf{r},t;\mathbf{Y}) = \frac{i\partial_t\beta_r}{\pi v|\beta|^2}\sqrt{\frac{(-Z_1-iF_1)(-Z_2-iF_2)}{(z_b-Z_1-iF_1)(z_b-Z_2-iF_2)}}\times$$
$$\overset{+}{\delta}\left[t-\bar{t}-t_p(\mathbf{r})-\tfrac{i}{2}T_p(\mathbf{r})\right] \tag{72}$$

where we define

$$t_p(\mathbf{r}) = v^{-1}(z_b + x_{b_1}^2/2R_1 + x_{b_2}^2/2R_2) \tag{73}$$
$$T_p(\mathbf{r}) = T + v^{-1}(x_{b_1}^2/I_1 + x_{b_2}^2/I_2) \tag{74}$$

Expression with (73)–(74) is readily identified as an astigmatic PB whose major axes are x_{b_1} and x_{b_2}.

Clearly, from (72), $t_p(\mathbf{r})$ is the paraxial propagation delay along the z_b axis, hence R_j are the wavefront radii of curvature in the x_{b_j} directions. $T_p(\mathbf{r})$ is the temporal half-amplitude length of $\overset{+}{\delta}$ pulse the and it is inversely proportional to the pulse amplitude. Thus the field is strongest on the beam axis where $T_p(\mathbf{r})$ is minimal and it decays as T_p grows away from the beam axis. The half-amplitude beam width in the x_{b_j} directions is found by solving $T_p(\mathbf{x}_{b_j}) = 2T_p(0)$, giving

$$D_j(z_b) = 2\sqrt{vTI_j(z_b)} \tag{75}$$

The collimation lengths in the (x_{b_j}, z) cross sectional planes are F_j and the waists are located at $z_b = Z_j$ with the corresponding widths $2\sqrt{vTF_j}$. From (75) with (71) one notes that in the collimation (Fresnel) zone $|z_b - Z_j| < F_j$, the PB is essentially unaffected by the propagation, whereas outside this zone, z_b opens up along a far field diffraction angle

$$\Theta_j = 2\sqrt{vT/F_j}. \tag{76}$$

As mentioned earlier, the propagator (72) belongs to the general class of PB fields in [5, 13]. An important feature of these solutions is that all their frequency components have the *same* collimation distance and radii of curvature (see (57)–(59) with β being frequency independent). This implies that the beam width in the $z = 0$ plane should be proportional to $\omega^{-1/2}$ (see (58)). Such wavepackets have been termed iso-diffracting [33] .

V. ILLUSTRATIVE EXAMPLE

V.1. The initial field

The spectral consideration for both the plane-wave spectrum and the local spectrum are illustrated here for a typical initial field distribution $u_o(\mathbf{x}, t)$,

$$u_o(\mathbf{x}, t) = \mathrm{Re}\ \overset{+}{\delta}(t - \tfrac{i}{2}T_o - \frac{i}{2}|\mathbf{x}|^2/v\alpha) \tag{77}$$

where $T_o > 0$ and $\alpha = \alpha_r + i\alpha_i$, with $\alpha_r > 0$, are parameters. The *real* distribution has the form (see (65))

$$u_o(\mathbf{x}, t) = \frac{1}{\pi} \frac{T_{p_o}/2}{(t - t_{p_o})^2 + (T_{p_o}/2)^2} \tag{78}$$

with (cf. (66))

$$t_{p_o}(\mathbf{x}) = \frac{1}{2} \frac{\alpha_i}{|\alpha|^2 v} |\mathbf{x}|^2, \qquad T_{p_o}(\mathbf{x}) = T_o + \frac{\alpha_r}{|\alpha|^2 v} |\mathbf{x}|^2. \tag{79}$$

For a given $\mathbf{x}$, it peaks at $t_{p_o}(\mathbf{x})$ and its pulse length and peak value are given respectively by $T_{p_o}(\mathbf{x})$ and $2/\pi T_{p_o}(\mathbf{x})$. The spatial half-amplitude width of this distribution is given by (see (67))

$$D_o = 2\sqrt{vT_o|\alpha|^2/\alpha_r} \tag{80}$$

This distribution is depicted in Fig. 8a for $\alpha = 1 - 4i$ and $T_o = 10^{-4}$.

The field radiated by the distribution in (77) is a pulse-beam which has the paraxial form (see (72))

$$u(\mathbf{r}, t) = \mathrm{Re}\, \frac{-i\alpha}{z - i\alpha}\ \overset{+}{\delta}[t - \tfrac{i}{2}T_o - v^{-1}(z + \tfrac{1}{2}|\mathbf{x}|^2/(z - i\alpha)]. \tag{81}$$

Following the analysis in (75), the waist of this PB field occurs at $z = -\alpha_i$ and its width there equals to

$$D_{\text{waist}} = 2\sqrt{vT_o\alpha_r} \tag{82}$$

V.2. Plane-wave spectrum

Applying the transient plane-wave transform (the slant stack transform) in (11) to (77), we obtain, exactly,

$$\widetilde{u}_o(\boldsymbol{\xi}, \tau) = \mathrm{Re}\,\{-2i\pi v\alpha\ \overset{+}{\delta}{}^{(-1)}(\tau - \frac{i}{2}T_o - \tfrac{i}{2}|\boldsymbol{\xi}|^2\alpha/v)\,\} \tag{83}$$

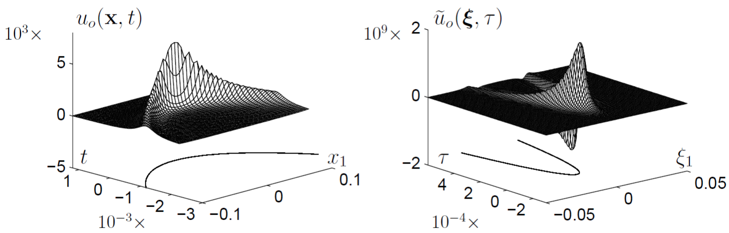

(a) (b)

Figure 8. The initial field distribution (77) for $\alpha = 1 - 4i$ and $T_o = 10^{-4}$. **(a)** Spatial distribution: The line full describes the pulse maximum at $t_{p_o}(\mathbf{x})$; **(b)** Spectral distribution of $\widetilde{u}''(\boldsymbol{\xi},\tau)$: The full line describes the spectral peak as found via the stationary point constraint and the Legendre transform

In this expression

$$\overset{+}{\delta}{}^{(-1)}(t) \equiv \int_{-1}^{t} \overset{+}{\delta}(t')dt' = 1 + (\pi i)^{-1} \ln t, \quad -\pi \leq \arg\{\ln t\} \leq 0 \quad (84)$$

is the analytic Heaviside (or unit step) function (i.e, Re $\overset{+}{\delta}{}^{(-1)}(t \text{ real}) = H(t)$). The resulting transient plane-wave propagator $-\partial_t^2 \widetilde{u}_o(\boldsymbol{\xi},\tau)$ (see (12)) is depicted in Fig. 8b.

To parameterize this expression we separate the argument of the $\overset{+}{\delta}$ function in (83) into real and imaginary parts. We then find that, for a given $\boldsymbol{\xi}$, the plane-wave spectrum peaks at $\tau = -\frac{1}{2}\alpha_i|\boldsymbol{\xi}|^2/v$. Its pulse-length and spectral ($\boldsymbol{\xi}$) width are given by $\widetilde{T} = T_o + |\boldsymbol{\xi}|^2\alpha_r/v$ and $\widetilde{D} = 2\sqrt{T_o v/\alpha_r}$, respectively. Note that the spectral width relates to D_{waist} of (82) via $\widetilde{D} = 4vT_o/D_{\text{waist}}$.

The exact spectral results in (83) and Fig. 8b can be readily explained in view of the spectral localization considerations in Sec. II.3, by noting that the distribution in (77) has the short-pulse form (17) with $\Phi_o(\mathbf{x}) = vt_{p_o}(\mathbf{x})$. We determine first the conditions under which these spectral localization considerations are valid. First it is required that the pulse length vT_o be much smaller than the spatial width D_o of (80). This directly implies that $\alpha_r/|\alpha|^2 \ll T_o$. Next we note from (20) that the wavefront radius of curvature of the data in the $(\mathbf{x}, vt)$ plane is given by $R_o = |\alpha|^2/\alpha_i$ hence from (20), the asymptotic contributing zone is given by $2\sqrt{vT_o\alpha_i/|\alpha|^2}$. Requiring that this zone will be much smaller than D_o of (80) we find that $\alpha_i \gg \alpha_r$. Clearly the two conditions above are compatible.

Having established the conditions for the asymptotic spectral localization of the data we may explain now the exact results in (83). For a given $\boldsymbol{\xi}$ the main contribution to $\widetilde{u}_o(\boldsymbol{\xi},\tau)$ is obtained from the *stationary delay* point (18) which gives here $\mathbf{x}_s(\boldsymbol{\xi}) = \boldsymbol{\xi}|\alpha|^2/\alpha_i$, and the peak in he spectrum is obtained from the Legendre transform (19) which gives here $\tau(\boldsymbol{\xi}) = -\frac{1}{2}|\boldsymbol{\xi}|^2|\alpha|^2/v\alpha_i$. Clearly if $\alpha_i \gg \alpha_r$ then $\tau(\boldsymbol{\xi}) \simeq -\frac{1}{2}\alpha_i|\boldsymbol{\xi}|^2/v$ which is the value of τ where the exact spectrum in (83) peaks. This line is also depicted in Fig. 8b.

V.3. Local spectrum

The time-dependent local spectrum of the initial distribution (77) is obtained via local Radon transform (36). Using also the Gaussian-δ window (65) and evaluating the integral in closed form we obtain

$$U_o(\mathbf{Y}) = \mathrm{Re}\frac{-2i\pi v}{\alpha^{-1}+\beta^{*-1}}\times \\ \overset{+}{\delta}{}^{(1)}\left[\bar{t} - \tfrac{i}{2}T_o - \tfrac{i}{2}T - (\beta^*\bar{\boldsymbol{\xi}}\cdot\bar{\mathbf{x}} + \tfrac{i}{2}|\bar{\mathbf{x}}|^2 + \tfrac{i}{2}\alpha\beta^*|\bar{\boldsymbol{\xi}}|^2)/v(\alpha+\beta^*)\right] \tag{85}$$

where from (62) $\overset{+}{\delta}{}^{(1)}(t) = -1/\pi i/t^2$. Henceforth we shall consider a window with no curvature i.e., with real β. Note that for $\beta \gg |\alpha|, |\bar{\mathbf{x}}|$ and $T \ll T_o$, expression (85) reduces to the transient plane-wave spectrum (83).

The phase-space location where the local spectrum is concentrated can be determined by minimizing the imaginary part of the argument of the δ function in (85). This defines a relation between $\bar{\mathbf{x}}$ and $\bar{\boldsymbol{\xi}}$. The value of $\bar{t}$ where the waveform in (85) peaks under this condition is found then by setting the real part of that argument to zero. For a given $\bar{\mathbf{x}}$ one thus finds

$$\bar{\boldsymbol{\xi}} = \frac{\bar{\mathbf{x}}\alpha_i}{\alpha_r\beta+|\alpha|^2}, \quad v\bar{t} = \frac{\alpha_i}{|\alpha+\beta|^2}\left(\frac{1}{2} + \frac{\beta(\beta+\alpha_r)}{|\alpha|^2+\alpha_r\beta} - \frac{\beta^2\alpha_i^2}{2(|\alpha|^2+\alpha_r\beta)^2}\right).$$

If now β is chosen so that $\beta \ll |\alpha|$ then this condition reduces to

$$\bar{\boldsymbol{\xi}} = \frac{\bar{\mathbf{x}}\alpha_i}{|\alpha|^2}, \quad \bar{t} = \frac{1}{2}|\bar{\mathbf{x}}|^2\frac{\alpha_i}{v|\alpha|^2}. \tag{86}$$

As expected this final result is independent of the window parameter β. The constraint in (86) is depicted in Fig. 9a (full line) for the initial field distribution with $\alpha = 1 - 4i$ shown in Fig. 8a. In view of the

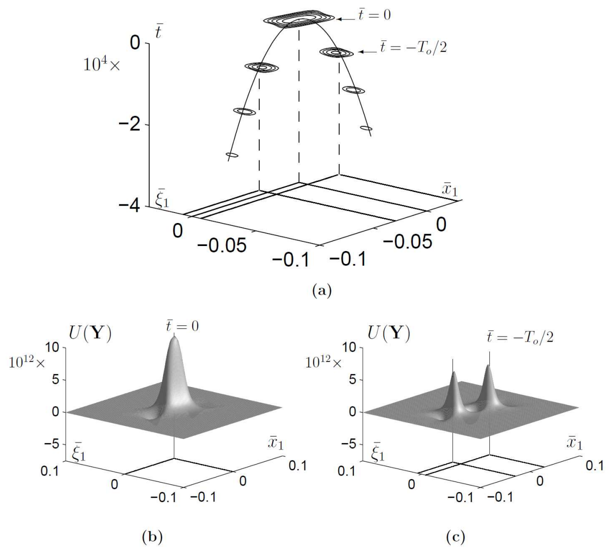

Figure 9. The local spectrum (85) for the field in Fig. 8a. **(a)** The phase-space radiation constraint. Contour plots of $U_o(\mathbf{Y})$ in cross sectional planes $\bar{t}/T_o = 0, -1/2, -1, -3/2$. The contour plots are concentrated about the radiation constraint (86) (full line). The contour levels are 0, 3db, 6db, 9db, 12db and 15db below the peak level of $U_o(\mathbf{Y})$ at $(\bar{\mathbf{x}}, \bar{\boldsymbol{\xi}}, \bar{t}) = (0, 0, 0)$. **(b)** and **(c)**: Snapshots of the local spectrum for $\bar{t} = 0$ and $\bar{t} = -T_o/2$, respectively. The spectrum is shown in the $(\bar{x}_1, \bar{\xi}_1)$ plane for $(\bar{x}_2, \bar{\xi}_2) = (0, 0)$. Window parameters: $\beta = 1$ and $T = 0$.

cylindrical symmetry of the initial field, the constraint is plotted in the $(\bar{x}_1, \bar{\xi}_1, \bar{t})$ domain for $(\bar{x}_2, \bar{\xi}_2) = (0, 0)$.

Expression (86) for the phase space localization of $U_o(\mathbf{Y})$ can readily be explained in terms of the general considerations in Sec. III.2.3. Indeed, using from (79) $\Phi_o(\mathbf{x}) = vt_{p_o}(\mathbf{x}) = \frac{1}{2}|\mathbf{x}|^2\alpha_i/|\alpha|^2$, we observe that (86) agrees with the *radiation constraint* as defined in general in (47).

To demonstrate this phase-space localization, we show in Fig. 9a contour plots of the function $U_o(\mathbf{Y})$ at several cross sectional planes $\bar{t}/T_o = 0, -1/2, -1, -3/2$ in the $\mathbf{Y}$ domain. One observes that $U_o(\mathbf{Y})$ is localized about the radiation constraint (86). To clarify the structure of $U_o(\mathbf{Y})$ we also show in Figs. 9b,c snapshots of the distribution of $U_o(\mathbf{Y})$ for two values of $\bar{t}$: $\bar{t} = 0$ and $\bar{t} = -T_o/2$. The distribution is depicted in the $(\bar{x}_1, \bar{\xi}_1)$ plane with $(\bar{x}_2, \bar{\xi}_2) = (0, 0)$. The initial data parameters are $\alpha = 1 - 4i$ and $T_o = 10^{-4}$. Consequently we choose

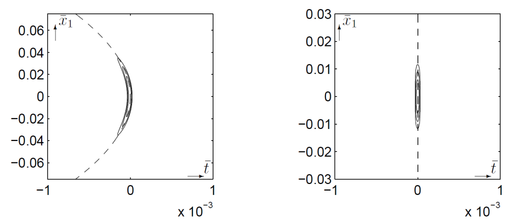

(a) (b)

Figure 10. The local spectrum (85) for the initial field in Fig. 8a, shown in a cross sectional plane $(\bar{x}_1, \bar{t})$ whereon $\bar{\boldsymbol{\xi}}$ is related to $\bar{x}_1$ via radiation condition (86). The contour lines at 3db, 6db and 9db below the peak are shown to be concentrated along the condition $\bar{t} = v_o^{-1}\Phi_o(\bar{\mathbf{x}})$ of (86) (dashed line). (**a**) $\alpha = 1 - 4i$ as in the examples in Figs. 8,9 and (**b**) $\alpha = 1$.

a window with $\beta = 1$ and $T \ll T_o$. We observe that indeed the distribution of the local spectrum is concentrated near the radiation constraint (86).

Finally in Fig. 10 we demonstrate the phase space localization from yet another point of view. The figure shows the contour lines of $U_o(\mathbf{Y})$ (85) sampled on a plane $(\bar{x}_1, \bar{t})$ defined by the radiation constraint $\bar{\boldsymbol{\xi}} = \bar{\mathbf{x}}\alpha_i/|\alpha|^2$ (see (86)). Two different cases of initial conditions are considered: (a) $\alpha = 1 - 4i$ (as in Figs. 8,9), and (b) $\alpha = 1$. One observes that the contour plots are concentrated along the constraint $\bar{t} = \frac{1}{2}|\bar{\mathbf{x}}|^2\alpha_i/v|\alpha|^2$ of (86) (dashed line).

It should be noted again that the plane-wave spectrum $\widetilde{u}_o(\boldsymbol{\xi}, \tau)$ can be localized in a ray-type local contributions as in (18)–(19) only if $\partial_{ij}\Phi_o(\mathbf{x})$ is large so that the asymptotic contributing zone (ACZ) in (20) is small. The local spectrum $U_o(\mathbf{Y})$ on the other hand is localized along the radiation constraint in (47) regardless of $\partial_{ij}\Phi_o(\mathbf{x})$. As an example, note that $U_o(\mathbf{Y})$ in Fig. 10(b) is localized along the constraint (86) even though $\alpha_i = 0$ here.

VI. SUMMARY

We presented a general phase-space framework for local modeling and analysis of radiation from extended source distribution in plane apertures. Both time-harmonic and TD representations have been considered. For short pulse fields, the TD representations are more efficient and physically incisive than the conventional transformation from the FD.

We considered and contrasted both *global* plane-wave representations (Sec. II) and *local* (windowed) phase-space representations (Secs. III and IV). The transient plane-wave spectrum is constructed by a slant stack (Radon) transform of the data in the $(\mathbf{x}, t)$ plane (see (11)). Using analytic signal theory, we obtained a unified representation which incorporates both the propagating and the evanescent spectrum (12), but the final result has also been expressed in term of real signals (13)–(16). It has also been demonstrated how the time-dependent spectrum could be localized about the space-time ray skeleton via a stationary delay evaluation of the plane-wave transform (see Fig. 3).

The general procedure for windowed phase-space representation has been described first using general window functions (Sec. III). Explicit expressions for Gaussian window functions have been developed next in Sec. IV. In each section we considered first the time-harmonic case and then the time-dependent representation. We shall summarize below the TD representations since they are more general than the frequency domain ones.

According to the general phase-space formulation, the transient field is expressed in (44) as a superposition of collimated pulsed-beam (PB) propagators $B(\mathbf{r}, t; \mathbf{Y})$ that emerge from all points $\bar{\mathbf{x}}$ in the source domain, in all directions $\bar{\boldsymbol{\xi}}$ and at all times $\bar{t}$, with $\mathbf{Y} = (\bar{\mathbf{x}}, \bar{\boldsymbol{\xi}}, \bar{t})$ representing the phase-space coordinates. This phase-space distribution of PBs is matched to the source distribution via the local spectral function $U_o(\mathbf{Y})$, obtained via a windowed slant-stack transform (or windowed Radon transform) of the data (36). As schematized in Fig. 4, this transform extracts the local space-time spectral information in the data, thereby enhancing only those PB propagators that emerge from a source along the local radiation direction. The resulting phase-space integral representations are therefore localized a priori about the physical ray skeleton of the data (see (47)). Further localization is due to the fact that only those PB that pass near a given space-time observation point actually contribute (see (48)).

Explicit expressions for the general phase-space operators mentioned above have been given in Sec. IV for the special case of the iso-diffracting Gaussian-δ window. This window yields well collimated PB propagators that could be tracked analytically through inhomogeneous medium or interactions with complicated boundaries [13, 15]. It also generates simple analytic expressions for the phase-space window operators. Thus the window kernel w and the PB propagators B are given, respectively, in (61)) and (69). The PBs are expressed conveniently in the (x_{b_1}, x_{b_2}, z_b) coordinate system of (52) that depend on the beam initiation point and direction. The physical parameters of the PBs, i.e., the pulse and beam widths, the collimation distance, etc., have been identified and discussed in (70)–(76).

The phase-space beam approach is currently being explored for local analysis of short-pulse scattering data and inverse scattering. Here the local analysis extracts the local directional information in the time-dependent data and matches pulsed-beams that are backpropagated to form the image of the scatterer [30]. It has further been found that the local PB spectrum of the data is directly related to the local Radon transform of the scattering object. This gives rise to several local backpropagation and inversion schemes.

Acknowledgments

This work is supported in part by the US-Israel Binational Science Foundation, Jerusalem, Israel, under grant No. 92–00273 and in part by the U.S. Air Force Office of Scientific Research, under Grant No. F49620-93-1-0093. The author expresses his thanks to Prof. Ehud Heyman for helpful discussions pertaining to the contents and preparation of the manuscript.

Appendix: Asymptotic evaluation for the beam fields

In order to analyze $\widehat{B}$ we shall express (29) with (50) in the form

$$\widehat{B}(\mathbf{r};\mathbf{X}) = \frac{k\beta}{2\pi}\, e^{ik\bar{\mathbf{x}}\cdot\bar{\boldsymbol{\xi}}} \int d^2\xi\, e^{ikq(\boldsymbol{\xi})}, \quad q(\boldsymbol{\xi}) = \boldsymbol{\xi}\cdot(\mathbf{x}-\bar{\mathbf{x}})+i|\boldsymbol{\xi}-\bar{\boldsymbol{\xi}}|^2\beta/2+\zeta z \tag{A.1}$$

where formal definition of the spectral integration domains is given in (3). Integral (A.1) has a stationary point $\boldsymbol{\xi}_s$ in the complex $\boldsymbol{\xi}$ domain, defined by

$$\nabla_\xi\, q = (\mathbf{x}-\bar{\mathbf{x}}) + i\beta(\boldsymbol{\xi}-\bar{\boldsymbol{\xi}}) - \boldsymbol{\xi}z/\zeta = 0 \ \text{ at } \ \boldsymbol{\xi} = \boldsymbol{\xi}_s. \tag{A.2}$$

This equation has a real solution $\boldsymbol{\xi}_s = \bar{\boldsymbol{\xi}}$ if and only if $\mathbf{X}$ and $\mathbf{r}$ are related by the observation constraint in (33) and $|\bar{\boldsymbol{\xi}}| < 1$. For all other values of $\mathbf{X}$ and $\mathbf{r}$, the solution of (2) is complex and can not be found explicitly. However, for points near the beam axis, an approximate expression can be obtained by a expanding $q(\boldsymbol{\xi})$ into a Taylor series about the beam direction $\bar{\boldsymbol{\xi}}$:

$$q(\boldsymbol{\xi}) = q_o + \mathbf{q}_1\cdot(\boldsymbol{\xi}-\bar{\boldsymbol{\xi}}) + \frac{1}{2}(\boldsymbol{\xi}-\bar{\boldsymbol{\xi}})\cdot\mathbf{q}_2\cdot(\boldsymbol{\xi}-\bar{\boldsymbol{\xi}}) \tag{A.3}$$

where

$$q_o \equiv q(\bar{\boldsymbol{\xi}}) = \bar{\boldsymbol{\xi}} \cdot (\mathbf{x} - \bar{\mathbf{x}}) + \bar{\zeta} z, \quad \bar{\zeta} = \sqrt{1 - |\bar{\boldsymbol{\xi}}|^2} \tag{A.4a}$$

$$\mathbf{q}_1 \equiv \nabla_\xi q\big|_{\bar{\boldsymbol{\xi}}} = (\mathbf{x} - \bar{\mathbf{x}}) - z\bar{\boldsymbol{\xi}}/\bar{\zeta} \tag{A.4b}$$

$$\mathbf{q}_2 \equiv \nabla_\xi \nabla_\xi q\big|_{\bar{\boldsymbol{\xi}}} = \begin{bmatrix} i\beta - z(\bar{\xi}_1^2 + \bar{\zeta}^2)/\bar{\zeta}^3 & -z\bar{\xi}_1\bar{\xi}_2/\bar{\zeta}^3 \\ -z\bar{\xi}_1\bar{\xi}_2/\bar{\zeta}^3 & i\beta - z(\bar{\xi}_2^2 + \bar{\zeta}^2)/\bar{\zeta}^3 \end{bmatrix} \tag{A.4c}$$

From (3), the stationary point is given by

$$\boldsymbol{\xi}_s = \bar{\boldsymbol{\xi}} - \mathbf{q}_2^{-1} \cdot \mathbf{q}_1 \tag{A.5}$$

and (A.1) yields

$$\widehat{B} \sim \widehat{B}_s = (\beta/\sqrt{\det \mathbf{q}_2}) e^{ik(\bar{\mathbf{x}} \cdot \bar{\boldsymbol{\xi}} + q_o - \frac{1}{2}\mathbf{q}_1 \cdot \mathbf{q}_2^{-1} \cdot \mathbf{q}_1)}. \tag{A.6}$$

Finally, utilizing the beam coordinates in (52) we find that the Taylor coefficients above are given by

$$q_o = z_b, \quad \mathbf{q}_1 = \begin{bmatrix} \bar{\zeta}\bar{\xi}_1/|\bar{\boldsymbol{\xi}}| + |\bar{\boldsymbol{\xi}}|\bar{\xi}_1/\bar{\zeta} & -\bar{\xi}_2/|\bar{\boldsymbol{\xi}}| \\ \bar{\zeta}\bar{\xi}_2/|\bar{\boldsymbol{\xi}}| + |\bar{\boldsymbol{\xi}}|\bar{\xi}_2/\bar{\zeta} & \bar{\xi}_1/|\bar{\boldsymbol{\xi}}| \end{bmatrix} \begin{bmatrix} x_{b_1} \\ x_{b_2} \end{bmatrix},$$
$$-\mathbf{q}_1 \cdot \mathbf{q}_2^{-1} \cdot \mathbf{q}_1 = \mathbf{x}_b \cdot \mathbf{Q} \cdot \mathbf{x}_b \tag{A.7}$$

where $\mathbf{Q}$ is given by (55). The final result (54) is obtained by substituting (A.7) into (6). From (5) and (A.7) we note that the displacement of $\bar{\boldsymbol{\xi}}_s$ from the real value $\bar{\boldsymbol{\xi}}$ is proportional to $\mathbf{x}_b$, thereby justifying the Taylor analysis above for observation points with small $|\mathbf{x}_b|$ near the beam axis.

REFERENCES

1. J.B. Brittingham, "Focus wave modes in homogeneous maxwell's equation: Transverse electric mode," *J. Appl. Phys.*, 5:1179–1189, 1983.
2. R.W. Ziolkowsky, "Localized transmission of electromagnetic energy," *Phys. Rev. A*, 39:2005–2033, 1989.
3. H.E. Moses and R.T. Prosser, "Initial conditions, sources and three dimensions. Part I: The inverse initial value problem. acoustic and electromagnetic 'bullets', expanding waves and imploding waves," *IEEE Trans. Antennas Propagat.*, 34:188–196, 1986.
4. T.T. Wu, "Electromagnetic missiles," *J. App. Phys*, 60:2981–2985, 1985.

5. E. Heyman and L.B. Felsen, "Complex source pulsed beam fields," *J. Opt. Soc. Am. A*, 6:806–817, 1989.
6. E. Heyman, B.Z. Steinberg, and R. Ianconescu, "Electromagnetic complex source pulsed beam fields," *IEEE Trans. Antennas Propagat.*, 38:957–963, 1990.
7. L.B. Felsen and N. Marcuvitz, *Radiation and Scattering of Waves*, Prentice-Hall, Englewood Cliffs, N.J., 1973.
8. L.B. Felsen, "Novel ways for tracking rays," *J. Opt. Soc. Am., A*, 2:954–963, 1985, Invited Paper.
9. C.H. Chapman, "A new method for computing synthetic seismograms," *Geophys. J. Roy. Astro. Soc*, 54:481–518, 1978.
10. E. Heyman and L.B. Felsen, "Weakly dispersive spectral theory of transients (STT), part I: Formulation and interpretation; part II: Evaluation of the spectral integral; part III: Applications," *IEEE Trans. Antennas Propagat.*, 35:80–86;574–580;1258–1266, 1987.
11. T. B. Hansen and A.D. Yaghjian, "Planar near-field scanning in the time-domain. Part I: Fomulation," *IEEE Trans. Antennas Propagat.*, 42:1280–1291, 1994.
12. T. B. Hansen and A.D. Yaghjian, "Planar near-field scanning in the time-domain. PartII: Sampling theorem and computation schemes," *IEEE Trans. Antennas Propagat.*, 42:1292–1300, 1994.
13. E. Heyman, "Pulsed beam propagation in an inhomogeneous medium," *IEEE Trans. Antennas Propagat.*, 42:311–319, 1994.
14. E. Heyman, R. Strachielevitz, and D. Kosloff, "Pulsed beam reflection and transmission at a planar interface: Exact solutions and approximate local models," *Wave Motion*, 18:315–343, 1993.
15. R. Ianconescu and E. Heyman, "Pulsed beam diffraction by a perfectly conducting wedge. Exact solution," *IEEE Trans. Antennas Propagat.*, 42:1377–1385, 1994.
16. V. Ĉerveny, M.M. Popov and I. Pŝenĉik, "Computation of wave fields in inhomogeneous media - Gaussian beam approach," *Geophys. J. Roy. Asro. Soc*, 70:109–128, 1982.
17. E. Heyman, "Complex source pulsed beam expansion of transient radiation," *Wave Motion*, 11:337–349, 1989.
18. M.J. Bastiaans, "The expansion of an optical signal into a discrete set of Gaussian beams," *optik*, 57:95–102, 1980.
19. P.D. Einziger, S. Raz, and M. Shapira, "Gabor representation and aperture theory," *J. Opt. Soc. Am. A*, 3:508–522, 1986.
20. B.Z. Steinberg, E. Heyman, and L.B. Felsen, "Phase space beam summation for time-harmonic radiation from large apertures," *J. Opt. Soc. Am. A*, 8:41–59, 1991.

21. J.J. Maciel and L.B. Felsen, "Systematic study of fields due to extended apertures by Gaussian beam discretization," *IEEE Trans. Antennas Propagat.*, 37:884–892, 1989.
22. A. Dendane and J.M. Arnold, "Scattered field analysis of a focused reflector using the Gabor series," *IEE Proc.- Microwaves, Antennas and Propagation*, 141:216–222, 1994.
23. J.M. Arnold, "Phase-space localization and discrete representations of wave fields," *J. Opt. Soc. Am. A*, 12:111–123, 1995.
24. B.Z. Steinberg, E. Heyman, and L.B. Felsen, "Phase space beam summation for time dependent radiation from large apertures: Continuous parametrization," *J. Opt. Soc. Am. A*, 8:943–958, 1991.
25. B.Z. Steinberg and E. Heyman, "Phase space beam summation for time dependent radiation from large apertures: Discretized parametrization," *J. Opt. Soc. Am. A*, 8:959–966, 1991.
26. B.Z. Steinberg and E. Heyman, "The local Radon transform and variable scale resolution with application to time-dependent radiation," *SIAM J. Appl. Math.*, 53:381–400, 1993.
27. A.E. Siegman, "Hermite-Gaussian functions of complex argument as optical-beam eigenfunctions," *J. Opt. Soc. Am.*, 63:1093–1094, 1973.
28. E. Heyman and I. Beracha, "Complex multipole pulsed beams and Hermite pulsed beams: A novel expansion scheme for transient radiation from well collimated apertures," *J. Opt. Soc. Am. A*, 9:1779–1793, 1992.
29. B.Z. Steinberg and J.J. McCoy, "Marching acoustic fields in a phase-space," *J. Acoust. Soc. Am.*, 93:188–204, 1993.
30. T. Melamed, *Phase-space techniques for time-domain local inversion of inhomogeneous medium*, PhD thesis, Tel-Aviv university, 1996.
31. C.H. Chapman, "Generalized Radon transforms and slant stacks," *Geophys. J.Roy.Astr. Soc.*, 66:445, 1981.
32. M.J. Bastiaans, "Signal descriptions by means of a local frequency spectrum," In *Transformation in Optical Signal Processing*, volume 373, pages 49–62, Proc. SPIE, 1981.
33. E. Heyman and T. Melamed, "Certain considerations in aperture synthesis of ultrawideband/short-pulse radiation," *IEEE Trans. Antennas Propagat.*, 42:518–525, 1994.